Supercond. Sci. Technol. **32** (2019) 015007 (9pp) https://doi.org/10.1088/1361-6668/aaee01

Thermal and magnetic strain measurements on a REBaCuO ring bulk reinforced by a metal ring during field-cooled magnetization

K Takahashi[1], S Namba[1], H Fujishiro[1], T Naito[1], Y Yanagi[2], Y Itoh[2] and T Nakamura[3]

[1] Department of Physical Science and Materials Engineering, Faculty of Science and Engineering, Iwate University, 4-3-5 Ueda, Morioka 020-8551, Japan
[2] IMRA Material R&D Co., Ltd, 2-1 Asahi-machi, Kariya 448-0032, Japan
[3] RIKEN, 2-1 Hirosawa, Wako 351-0198, Japan

E-mail: fujishiro@iwate-u.ac.jp

Received 14 July 2018, revised 26 October 2018
Accepted for publication 2 November 2018
Published 29 November 2018

Abstract

We have measured the mechanical strain, $\varepsilon_\theta = dL_\theta/L_\theta$, using strain gauges adhered along the circumferential (θ) direction on the EuBaCuO ring bulk reinforced by an aluminum alloy ring during the cooling process from 289 K to 50 K, and during field-cooled magnetization (FCM) at 50 K under magnetic fields from $B_{app} = 5.3$ and 6.3 T. To discuss the mechanical reinforcement effect of the aluminum alloy ring and the magnetic strain during FCM, we have performed numerical simulations using the finite element method for the ring bulk assuming realistic superconducting characteristics. The experimental results of the thermal strain during the cooling process, $\varepsilon_\theta^{cool} = dL_\theta^{cool}/L_\theta$, from 289 K to 50 K on the bulk surface validated our numerical results, in which the $\varepsilon_\theta^{cool}$ value became smaller at the outer edge, compared to that at the inner edge of the bulk surface. These results strongly suggest an inhomogeneous reinforcement of the bulk due to the difference in the thermal contraction along the height direction between the ring bulk and the outer Al alloy ring with finite height. The experimental results of the time step dependence of the magnetic strain during FCM, $\varepsilon_\theta^{FCM} = dL_\theta^{FCM}/L_\theta$, were reproduced qualitatively by the numerical simulation. The measurement of mechanical strain is effective to clarify the reinforcement effect of the metal ring during cooling and the mechanical stress during FCM.

Keywords: mechanical strain, field cooled magnetization, REBaCuO bulk, shrink fit steel, numerical simulation, strain gauge measurement

(Some figures may appear in colour only in the online journal)

1. Introduction

RE-Ba-Cu-O (REBaCuO, RE: rare earth element or Y) bulk superconductors have been developed from viewpoints of trapped field enhancement, including the critical current density, J_c, and the enlargement of sample size [1, 2]. As a result, such bulks with increased J_c can provide a compact and strong magnetic field source as a high-field trapped field magnet (TFM) capable of generating several Tesla. To date, the highest trapped field of 17.6 T has been achieved at 26 K in a disk-shaped GdBaCuO bulk pair reinforced by shrink-fit stainless streel [3]. A ring-shaped REBaCuO bulk superconductor is also considered useful for practical applications, such as nuclear magnetic resonance (NMR) spectrometers and magnetic resonance imaging (MRI) apparatus [4–8]. Trapped field enhancement in a bulk superconducting NMR/MRI system is an ongoing challenge to improve its resolution.

To give the best indication of the trapped field capability of a TFM, field-cooled magnetization (FCM) is commonly used. Although the trapped field value of REBaCuO bulks, which can be estimated from its $J_c(B, T)$ characteristics, could be over 20 T at 20 K [9], the mechanical strength of such

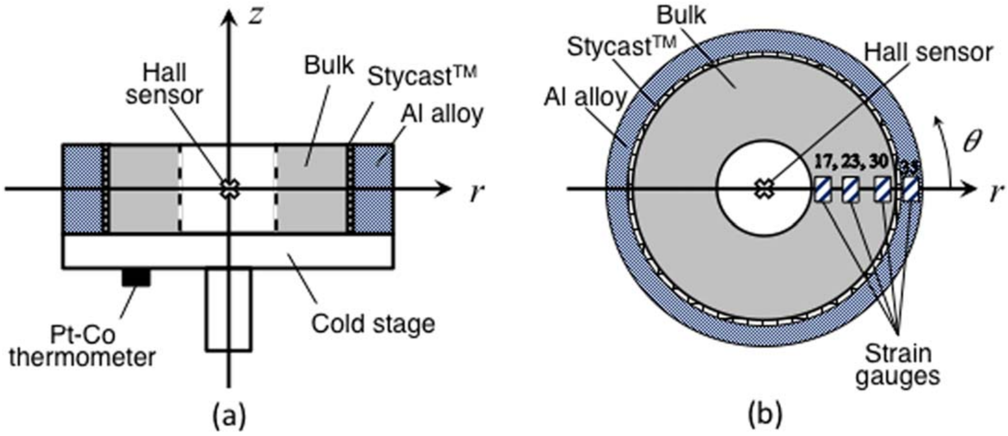

Figure 1. (a) Measuring position of the central magnetic field, $B_z(t)$, using a Hall sensor. (b) Plan view of the bulk surface, on which four strain gauges were adhered on the ring bulk and Al alloy ring in an array at $r = 17$, 23, 30 and 35 mm to measure the strain along the θ-direction.

brittle ceramic materials restricts the realistic maximum trapped field value. When the bulk is magnetized by FCM, the bulk could sustain and trap some of the applied field by an induced supercurrent flowing around the vortex pinning centers within the bulk. Meanwhile, during its magnetization process, large Lorentz forces ($\boldsymbol{J} \times \boldsymbol{B}$) are generated due to the interaction between induced current density (J) and magnetic field (B), and results in fracture of the sample when the magnetic stress exceeds the mechanical strength of the bulk material. In any case, cracks propagate along the radial direction [10, 11], and the principal hoop stress is applied along the circumferential direction of the bulk during FCM. The tensile strength of REBaCuO bulks is as low as 50 MPa along the *ab*-plane [12], which depends on the existence of imperfections inside the bulk, such as grain boundaries, cavities and micro-cracks [13]. Silver (Ag) addition is an effective way as an internal reinforcement technique to reduce numbers of cavities, and hence, improves the fracture strength up to 70 MPa [14–16]. On the other hand, as an external reinforcement technique, several kinds of metal ring fitting have been applied to the disk and ring bulks, which is expected to apply a compressive stress to the bulk under the cooling process (before magnetization) due to the difference of the thermal contraction coefficient between the bulk and metal ring [3, 5]. The acknowledgement of such a reinforcement effect has become more crucial to avoid the fracture of the bulk, in parallel with the enhancement of the trapped field.

We have reported the numerical simulation results of the mechanical stress behaviors in the REBaCuO ring bulk with finite height reinforced by a metal ring during FCM [17, 18]. We also mentioned the weakness in such conventional reinforcement techniques using a metal ring, in which an inhomogeneous stress profile with a positive tensile stress occurs at the outer edge of the bulk surface owing to the larger thermal contraction of the metal ring with finite height along both radial and height directions, compared to that of the bulk [18]. In these numerical models, the electromagnetic and mechanical parameters are assumed to be isotropic and homogeneous inside the bulk for simplicity. In addition, the interface between the outer bulk surface and inner metal ring surface was assumed to be fixed perfectly. Such numerical results of mechanical behavior should be validated and compared with actual experimental results.

A mechanical strain can be measured directly by a strain gauge adhered on the bulk surface in actual experiments [11]. The mechanical stress can be estimated by the strain measurements using Hooke's law and compared to the results of the numerical simulations. We would mention that the direct strain measurement is necessary to evaluate the reinforcement effect of a metal ring and the electromagnetic strain on the bulk surface.

In this paper, we measured the thermal strain, $\varepsilon_\theta^{cool} = dL_\theta^{cool}/L_\theta$, along the circumferential (θ) direction on the bulk surface during the cooling process from 289 K to 50 K to evaluate the reinforcement effect by aluminum alloy ring. We also measured the magnetic strain, $\varepsilon_\theta^{\mathrm{FCM}} = dL_\theta^{\mathrm{FCM}}/L_\theta$, along the θ-direction on the bulk surface at 50 K during FCM under magnetic fields from 5.3 and 6.3 T. The experimental results were compared with the numerical results. The strain measurement technique using a strain gauge could be applicable for evaluation of the mechanical reinforcement effect and the magnetic strain during FCM.

2. Experimental procedure and results

A EuBaCuO ring bulk with 10 wt% Ag of 64 mm in outer diameter (OD), 28 mm in inner diameter (ID), and 20 mm in height (H), was fabricated by the melt-processing method under atmosphere by Nippon Steel and Sumitomo Metal [19, 20]. The EuBaCuO ring bulk can achieve higher trapped field and higher magnetic field homogeneity with its low relative magnetic permeability ($\mu = 1.0013$), compared with that of GdBaCuO bulk ($\mu = 1.0194$) [5], which is preferable for NMR/MRI bulk magnets. The ring bulk was mounted in an aluminum (Al) alloy (A7075-T6) ring 5 mm in width (74 mm in OD and 64.1 mm in ID) with the same height as the ring bulk using Stycast™ 1266 resin. Figure 1(a) shows the experimental setup of the bulk and the measuring position of the magnetic field around the ring bulk. The bottom surface of the ring bulk with Al alloy ring was thermally connected to the cold stage of a Gifford–McMahon cycle helium refrigerator using an indium sheet in a vacuum chamber. The temperature of the bulk was controlled by a Pt–Co thermometer attached to the bottom surface of the cold stage. In the FCM process, the ring bulk was cooled to the magnetizing temperature of $T_s = 50$ K under the initial applied fields of $B_{app} = 5.3$ and 6.3 T, using a cryo-cooled superconducting solenoid magnet (JASTEC JMTD-10T100), and then, the external field was decreased linearly at -0.222 T min^{-1} down to zero. The time step (TS) of the descent of the magnetic field during FCM is defined as follows

$$\mathrm{TS} = 10\frac{B_{app} - B_{ex}}{B_{app}}, \tag{1}$$

where B_{ex} is the actual external field. The TS dependence of the local field, $B_z(t)$, along the z-direction was measured at the center of the bulk annuli using a Hall sensor (F. W. Bell, BHA 921). Figure 1(b) shows the schematic view of the top surface of the ring bulk. Four strain gauges (Tokyo Sokki, CFLA-1-350-11, (gauge length: 1 mm, gauge resistance: 350 Ω, gauge factor: $F = 2.09$) were adhered in an array along the θ-direction at $r = 17$, 23, 30 mm on the bulk surface and at $r = 35$ mm on the Al alloy ring surface using an epoxy adhesive (Tokyo Sokki, EA-2A) to measure the strain. The mechanical strain, $\varepsilon_\theta = dL_\theta/dL$, including the thermal contraction strain under the cooling process, $\varepsilon_\theta^{cool} = dL_\theta^{cool}/L_\theta$, and the electromagnetic expansion strain during FCM, $\varepsilon_\theta^{\mathrm{FCM}} = dL_\theta^{\mathrm{FCM}}/L_\theta$, is expressed by the following equation

$$\varepsilon_\theta = \frac{dL_\theta}{L_\theta} = \frac{L_\theta(T,\ B) - L_\theta}{L_\theta} = \frac{1}{F}\frac{dR}{R}, \tag{2}$$

where $dL_\theta = L_\theta(T,\ B) - L_\theta$ is the change of length along the θ-direction by temperature or magnetic field, $L_\theta = 2\pi r$ is the original length of the bulk along the θ-direction and r is the radial measurement position on the bulk surface. The $\varepsilon_\theta = dL_\theta/L_\theta$ value on the bulk sample was calculated by the ratio of dR/R shown in equation (2), where R (=350 Ω) is the initial resistance of the strain gauge and dR is the change in the resistance due to the mechanical strain under temperature or magnetic field variation. The temperature dependence of the electrical resistance, $R(T)$, of the strain gauge adhered on the quartz plate was measured from 300 K to 50 K by the four terminal method applying a constant current of 0.3 mA, which were used as the calibrated value. The magnetic field dependence of the electrical resistance, $R(B)$, of the strain gauge adhered on the quartz plate was also measured up to 10 T at 50 K, in which there was no need to calibrate the gauge resistance under the magnetic field. We have measured the gauge resistance, $R(T,\ B)$, adhered on the bulk several times, which were confirmed to be nearly the same values under the identical condition. We have also measured the temperature dependence of the thermal strain, $\varepsilon(T)$, of high-purity copper from 300 K to 50 K using the same method, in which the deviation from the recommended $\varepsilon_0(T)$ value, $(\varepsilon_0(T)$-$\varepsilon(T))/\varepsilon_0(T)$, was confirmed to be within 2%.

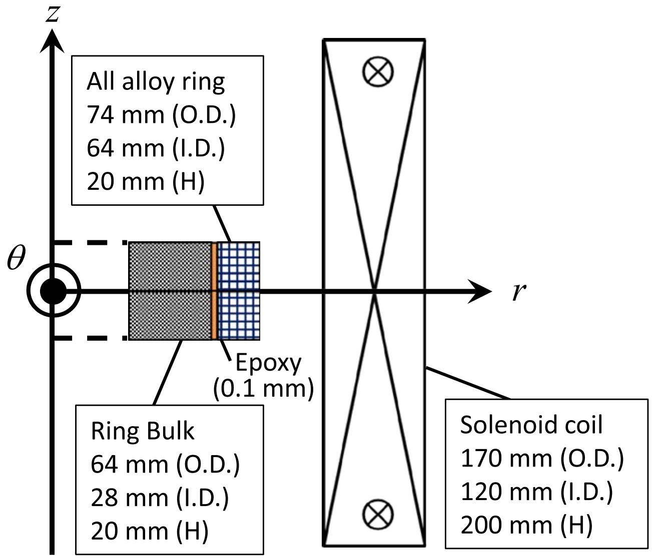

Figure 2. Cross-sectional view of the three-dimensional numerical model of the ring bulk reinforced by Al alloy ring (A7075-T6), magnetized using a solenoid coil.

3. Numerical simulation framework

To discuss the reinforcement effect of the metal ring and the magnetic strain during FCM in detail, we calculated both the thermal strain under cooling process, $\varepsilon_\theta^{cool}$, and the magnetic strain during FCM, $\varepsilon_\theta^{\mathrm{FCM}}$, using numerical simulations. We constructed a three-dimensional (3D) finite element model based on the actual experimental setup for FCM as shown in figure 2. The ring bulk with the same size as that used for the experiment was magnetized using a solenoid coil (170 mm in OD, 120 mm in ID and 200 mm in H), which is similar to previous work [18]. The ring bulk and the Al alloy ring were assumed to be fixed perfectly through an epoxy resin layer with 0.1 mm in thickness to reproduce the experimental condition.

Electromagnetic phenomena during FCM are described by the fundamental equation as follows [8, 21]

$$\nabla \times (\mu^{-1}\nabla \times \boldsymbol{A}) = J_0 - J, \tag{3}$$

where $\boldsymbol{A}$ is the magnetic vector potential, J_0 is the coil current density, J is the induced current density in the superconducting bulk, and μ is the magnetic permeability for the EuBaCuO ring bulk. The E–J power law was assumed to describe the nonlinear electrical properties of the superconducting bulk as follows

$$E = E_c\left(\frac{J}{J_c}\right)^n, \tag{4}$$

where E_c (= 10^{-4} V m^{-1}) is the characteristic electric field and n (= 20) is an appropriate value for the bulk superconductor [21]. The $J_c(B)$ characteristics of the bulk used in the simulation were determined using the following equation [22–24], for bulk superconducting materials exhibiting a

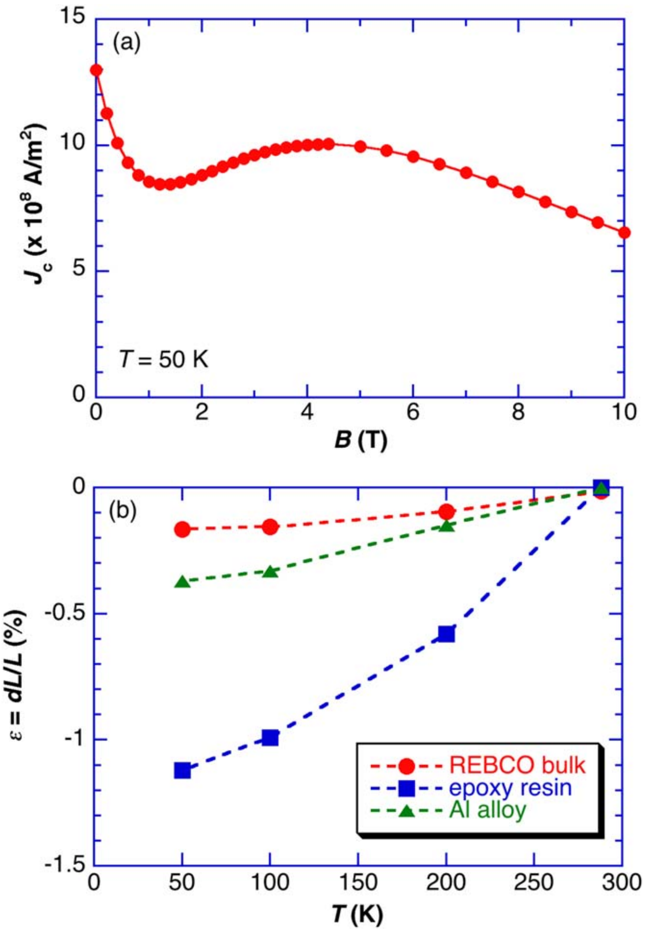

Figure 3. (a) Magnetic field dependence of the critical current density, $J_c(B)$, of the EuBaCuO bulk used in the numerical simulations. (b) Temperature dependence of the thermal contraction strain, $\varepsilon = dL/L$, of each material from 289 K to 50 K for mechanical simulation during the cooling process, which was linearly approximated in three temperature regions ($289\text{ K} \geqslant T \geqslant 200\text{ K}$, $200\text{ K} \geqslant T \geqslant 100\text{ K}$, $100\text{ K} \geqslant T \geqslant 50\text{ K}$).

Table 1. Numerical parameters for the $J_c(B)$ characteristics of the present bulk for equation (5).

	J_{c1} (A m^{-2})	B_L (T)	J_{c2} (A m^{-2})	B_{max} (T)	k
Present bulk	1.3×10^9	0.8	1.0×10^9	4.5	1.0

fishtail shape in their magnetization loop.

$$J_c(B) = J_{c1}\exp\left(-\frac{B}{B_L}\right) + J_{c2}\frac{B}{B_{max}}\exp\left[\frac{1}{k}\left(1-\left(\frac{B}{B_{max}}\right)^k\right)\right]. \quad (5)$$

Each parameter, which was determined by the fitting, is shown in table 1, and the $J_c(B)$ curve used in the simulation is shown in figure 3(a). The parameters of J_{c1} and J_{c2} used for the present simulation of the EuBaCuO bulk were determined as to reproduce the TS dependence of the trapped field, $B_z(t)$, obtained from actual experiment, as shown in the later section 4.2 in detail.

Table 2. Mechanical parameters (Young's modulus, E_Y, and Poisson ratio, ν) of EuBaCuO bulk, epoxy resin, and Al alloy (A7075-T6) used in the numerical simulation.

	EuBaCuO bulk	Epoxy resin	Al alloy (A7075-T6)
E_Y (GPa)	100	3	78
ν	0.33	0.37	0.34

In the numerical FCM process, the ring bulk was cooled to 50 K in fields of $B_{app} = 5.3$ and 6.3 T, and then, the external field, B_{ex}, was decreased linearly to 0 T at -0.222 T min^{-1} over ten steps. The temperature variation during FCM was ignored for simplicity, i.e. $Q = \boldsymbol{E}\cdot\boldsymbol{J} = 0$. The commercial FEM software package Photo-Eddy (Photon Ltd, Japan) was adapted for the analysis of the trapped field, B_z, perpendicular to the bulk surface, and induced current density, J_θ, along the θ-direction in the bulk. Elastic behavior in an isotropic material can be explained by Hooke's law, in which the stress tensor, σ_{ij}, is linearly proportional to the strain tensor, ε_{ij}, as follows

$$\sigma_{ij} = \lambda\cdot\varepsilon_{kk}\cdot\delta_{ij} + 2G\cdot\varepsilon_{ij}, \quad (6)$$

$$\lambda = \frac{E_Y\cdot\nu}{(1+\nu)(1-2\nu)}, \quad (7)$$

$$G = \frac{E_Y}{2(1+\nu)}, \quad (8)$$

where λ and G represent Lame's constants, δ_{ij} is the Kronecker delta function, E_Y is the Young's modulus, and ν is the Poisson ratio. The nodal force on each node of the meshed elements calculated by Photo-Eddy was imported to the commercial software package Photo-ELAS (Photon Ltd, Japan) for the analysis of the magnetic strain during FCM, $\varepsilon_\theta^{FCM} = dL_\theta^{FCM}/L_\theta$, due to the current-field interaction at each step of FCM. The mechanical parameters, E_Y and ν, of each component used in the mechanical simulation are summarized in table 2, which are assumed to be isotropic and to be in the elastic region. Figure 3(b) shows the temperature dependence of the thermal contraction strain, $\varepsilon = dL/L$, of each material from 289 K to 50 K, in which the dL/L value was linearly approximated in three temperature regions ($289\text{ K} \geqslant T \geqslant 200\text{ K}$, $200\text{ K} \geqslant T \geqslant 100\text{ K}$, $100\text{ K} \geqslant T \geqslant 50\text{ K}$). The thermal contraction coefficient, α, of each material at each temperature region was estimated from the gradient of the dL/L value shown in figure 3(b). The thermal strain in the ring bulk and Al alloy ring, $\varepsilon_\theta^{cool} = dL_\theta^{cool}/L_\theta$, which was produced by the difference in α between the bulk and the Al alloy ring, was calculated under cooling process, separately from the FCM process.

4. Experimental and numerical results

4.1. Cooling process

In this subsection, we focus on the external reinforcement effect by the Al alloy ring from the viewpoints of both the experimental and numerical results. Figure 4(a) shows the experimental results of the temperature dependence of the thermal strain under the cooling process, $\varepsilon_\theta^{cool}$, at each measurement position on the top

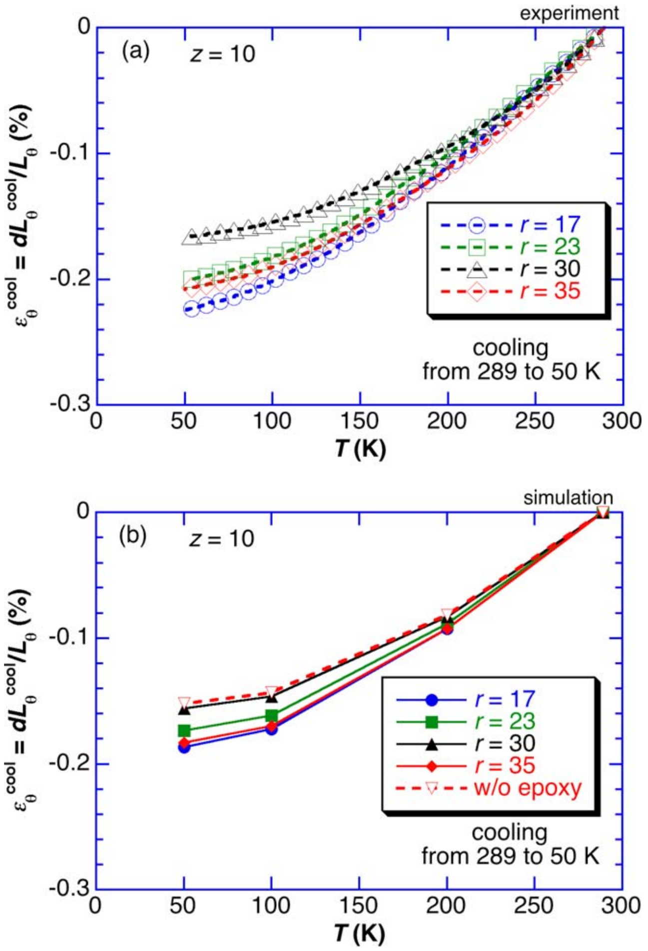

Figure 4. (a) Experimental and (b) numerical results of the temperature dependence of the thermal strain under the cooling process from 289 K to 50 K, $\varepsilon_\theta^{cool} = dL_\theta^{cool}/dL_\theta$, at each measurement position on the top surface of the ring bulk and the Al alloy ring. The $\varepsilon_\theta^{cool}$ profile for the ring bulk without reinforcement by the Al alloy ring (w/o epoxy) was also shown in (b).

surface of the bulk and the Al alloy ring. The bulk and the Al alloy ring start to shrink from 289 K gradually, and the $\varepsilon_\theta^{cool}$ value becomes negative with decreasing temperature. The negative $\varepsilon_\theta^{cool}$ value at $r = 17$ mm is the largest, meaning the highest compressive strain and decreases with increasing r in the bulk. The negative $\varepsilon_\theta^{cool}$ value on the Al alloy ring ($r = 35$ mm) showed slightly larger compressive strain than that at $r = 23$ mm. Figure 4(b) shows the numerical results of the temperature dependence of the $\varepsilon_\theta^{cool}$ profile at each position. The position and temperature dependences of the $\varepsilon_\theta^{cool}$ profile reproduce the experimental results well. In figure 4(b), the temperature dependence of the $\varepsilon_\theta^{cool}$ profile for the bulk is also shown, in which there is no epoxy resin at the interface (w/o epoxy). This result shows the $\varepsilon_\theta^{cool}$ profile of the bulk without any reinforcement by the metal ring, which was independent of the measurement position. The experimental results shown in figure 4(a) suggest that the thermal strain under cooling is affected by the Al alloy ring reinforcement and that the cooling strain changes depending on the measurement position.

Figure 5(a) shows the comparison of the cooling strain on the surface of the bulk ($z = 10$), $\varepsilon_\theta^{cool}$, between experimental and numerical results at 200, 100 and 50 K, as function of radius, r, of the bulk. The results were extracted from figure 4. Under the cooling process, both the bulk and the Al alloy ring contracted and the $\varepsilon_\theta^{cool}$ value became a negative value from 289 K to 200 K, 100 K and 50 K. The simulation results of the r-dependence of the $\varepsilon_\theta^{cool}$ profile and the absolute $\varepsilon_\theta^{cool}$ value reproduced the experimental ones at each temperature. The $\varepsilon_\theta^{cool}$ value decreased with increasing r in the bulk region (14 mm $< r <$ 32 mm) at each temperature, and the slope of the $dL_\theta^{cool}/dL_\theta$ profile also became steep with decreasing temperature. And then, the $\varepsilon_\theta^{cool}$ value negatively increases on the Al alloy ring region (32 mm $< r <$ 37 mm). Figure 5(b) shows the simulation results of the cooling strain, $\varepsilon_\theta^{cool}$, at 50 K, as function of radius for various conditions. The experimental and numerical $\varepsilon_\theta^{cool}$ profiles on the bulk surface ($z = 10$ mm) with the epoxy resin layer at 50 K are also shown again for reference. For the numerical $\varepsilon_\theta^{cool}$ profile without the epoxy resin layer (w/o epoxy) in the gap with 0.1 mm between the outer ring bulk and inner Al alloy ring, the $\varepsilon_\theta^{cool}$ value is -0.151% in the bulk region and this is independent of the z value. This behavior indicates that the ring bulk and Al alloy ring shrink freely and independently during the cooling process, i.e. the thermal compressive stress $\sigma_\theta^{cool} = 0$. On the other hand, for the numerical $\varepsilon_\theta^{cool}$ profile on the central axis of the bulk ($z = 0$ mm) with epoxy resin layer in the gap, the $\varepsilon_\theta^{cool}$ value slightly increases to -0.21% at $r = 14$ mm and -0.185% at $r = 30$ mm. This result suggests that the thermal reinforcement is effectively applied by the Al alloy ring. However, for the numerical $\varepsilon_\theta^{cool}$ profile on the bulk surface ($z = 10$ mm) with the epoxy resin layer, the $\varepsilon_\theta^{cool}$ value exhibits a moderate slope and reproduces the experimental results. These results indicate that the bulk is difficult to shrink along the θ-direction on the top surface of the bulk with increasing r.

Figures 5(c) and (d), respectively, show a schematic view of the displacement, dr and dz, along the r- and z-directions during cooling from 289 to 50 K, where the epoxy resin layer exists in the interface between the ring bulk and Al alloy ring. In figure 5(c) along the r-direction, the shrink measured on the top and bottom surfaces is smaller than that at the bulk center. On the other hand, along the z-direction, as shown in figure 5(d), the shrink on the bulk surface is smaller than that on the Al alloy ring. These results suggest that the thermal shrink in the bulk is not homogeneous due to the larger thermal contraction of the Al alloy ring with finite height, where the outer periphery of the ring bulk was pulled toward $z = 0$.

Figures 6(a) and (b), respectively, show the numerical results of the thermal stress profile after the cooling process, σ_θ^{cool}, along the θ-direction and σ_r^{cool}, along the r-direction inside the bulk and the Al alloy ring for various height positions from the center ($z = 0$ mm) to the top surface ($z = 10$ mm). In our previous study, we have reported the numerical results of the thermal stress, σ_θ^{cool}, and the thermal displacement profile under the cooling process in the bulk

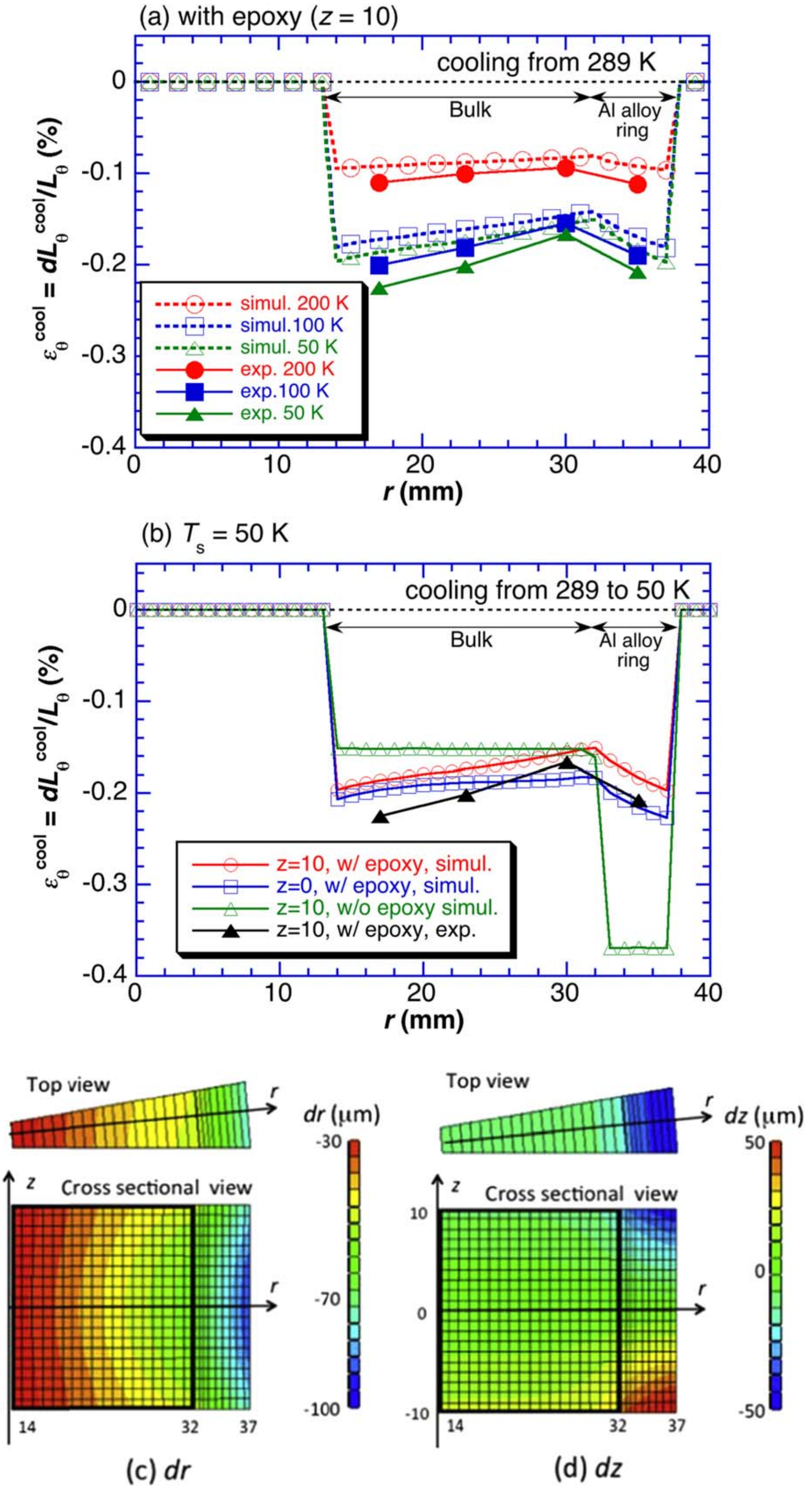

Figure 5. (a) Thermal strain profile during the cooling process, $\varepsilon_\theta^{cool} = dL_\theta^{cool}/L_\theta$, on the top surface at each temperature, 200 K, 100 K and 50 K, cooling from 289 K, comparing the numerical simulation results with the experimental results. (b) The $\varepsilon_\theta^{cool}$ profile under the cooling process, in which the no epoxy layer exists and both the ring bulk and Al alloy ring shrink independently. Schematic view of the displacement profile of the ring bulk under the cooling process along the (c) *r*- and (d) *z*-direction.

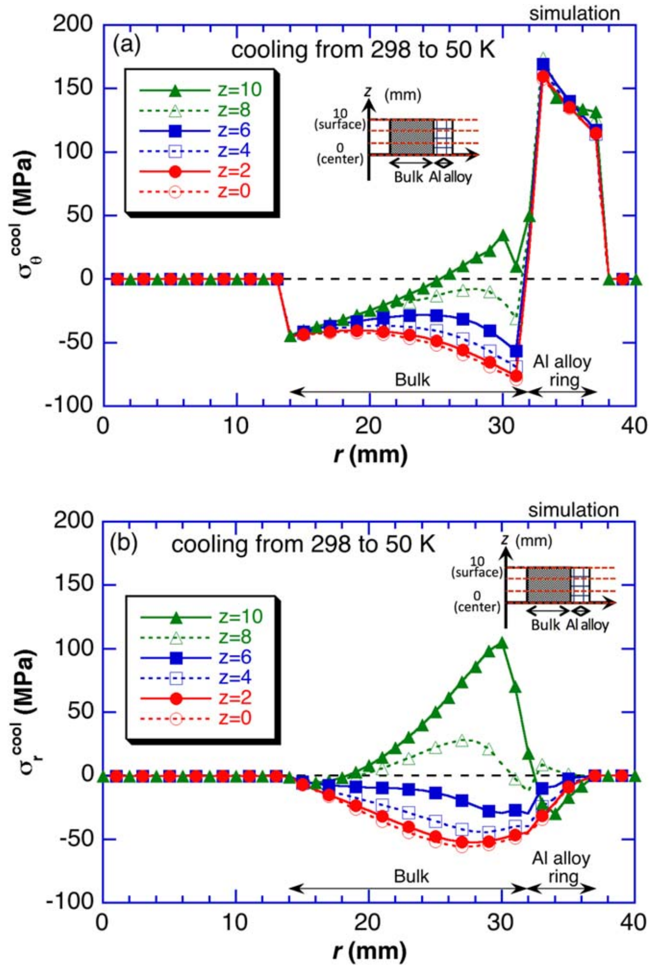

Figure 6. Numerical results of the thermal stress profiles inside the bulk and Al alloy ring after the cooling process from 289 K to 50 K, for (a) σ_θ^{cool}, along the θ-direction and (b) σ_r^{cool}, along the r-direction for various height (z-) positions (z = 0–10 mm).

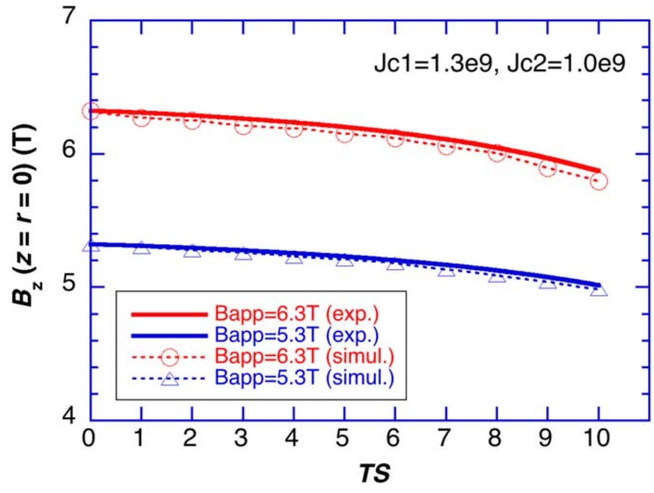

Figure 7. Experimental and numerical results of time step dependence of the magnetic field, B_z ($z = r = 0$ mm) at 50 K at the center of the ring bulk during FCM from B_{app} of 5.3 and 6.3 T.

reinforced by a metal ring, in which the stress profile might be inhomogeneous inside the bulk due to the finite height of the bulk and metal ring [17, 18]. In figure 6(a), it was also confirmed that the inhomogeneity of σ_θ^{cool} exists along the z-direction inside the bulk, in which the compressive σ_θ^{cool} decreased with increasing z and changed to the positive (tensile) value of +32 MPa at the outer edge of the bulk surface ($r = 30$ mm, $z = 10$ mm). In figure 6(b), the tensile σ_r^{cool} stress is also enhanced at the bulk surface ($z = 10$ mm), which is as large as +100 MPa. The present experimental results shown in figures 4 and 5 are partially reflected by such inhomogeneous stresses in conventional reinforcement using a relatively thin metal ring with the same height as the bulk. Recently, we have reported the wider metal ring is effective to reduce the electromagnetic expansive stress during FCM and to enhance the thermal compressive stress under cooling [18]. Note again that the present numerical simulation assumes that the epoxy resin layer is in the elastic region and is not broken or cracked. The experimental measurement of $\varepsilon_\theta^{cool}$, shown in figures 4 and 5, was limited only along the θ-direction and only on the bulk surface ($z = 10$ mm), although the actual stress distribution must be obtained from 3D strain variation. There might be a slight difficulty to estimate the thermal stress profile inside the bulk, except when using numerical simulations.

4.2. FCM process

In the case of the FCM process, we firstly describe the electromagnetic behavior of the trapped field, and then refer to the mechanical behavior. Figure 7 shows experimental results of the TS dependence of the field, B_z ($z = r = 0$ mm), at 50 K at the center of the ring bulk during FCM from $B_{\mathrm{app}} = 5.3$ and 6.3 T. For each B_{app}, the B_z value slightly decreased with increasing TS and then settled to the final value. Final trapped fields of $B_{\mathrm{T}} = 5.02$ and 5.87 T were successfully achieved at the tenth step after FCM from $B_{\mathrm{app}} = 5.3$ and 6.3 T, respectively. The numerical results of the TS dependence of the B_z ($z = r = 0$ mm) are also shown in figure 7, in which the parameters for the $J_{\mathrm{c}}(B)$ profile shown in table 1 were used in the simulation. The experimental B_z ($z = r = 0$ mm) profiles can be reproduced by the numerical simulation. These results suggest that the magnetic field dependence of the average critical current density, $J_{\mathrm{c}}(B)$, can be decided by the numerical fitting of the TS dependence of the trapped field, B_z(TS), to the experimentally obtained B_z(TS), which was measured at the center of the ring bulk. The ring bulk was not broken for applied fields up to 6.3 T and the final trapped field almost linearly increased with increasing B_{app}. These results suggest that the ring bulk was not fully magnetized during FCM and that the induced supercurrent flowed only in the outer and top and bottom regions of the ring bulk.

Figures 8(a) and (b) show experimental results of the TS dependence of the magnetic strain, $\varepsilon_\theta^{\mathrm{FCM}} = dL_\theta^{\mathrm{FCM}}/L_\theta$, at 50 K during FCM from $B_{\mathrm{app}} = 5.3$ and 6.3 T, respectively, at each measurement position on the bulk surface. The numerical results of the TS dependence of the $\varepsilon_\theta^{\mathrm{FCM}}$ value on the bulk surface ($z = 10$ mm) are also shown in each figure. Both

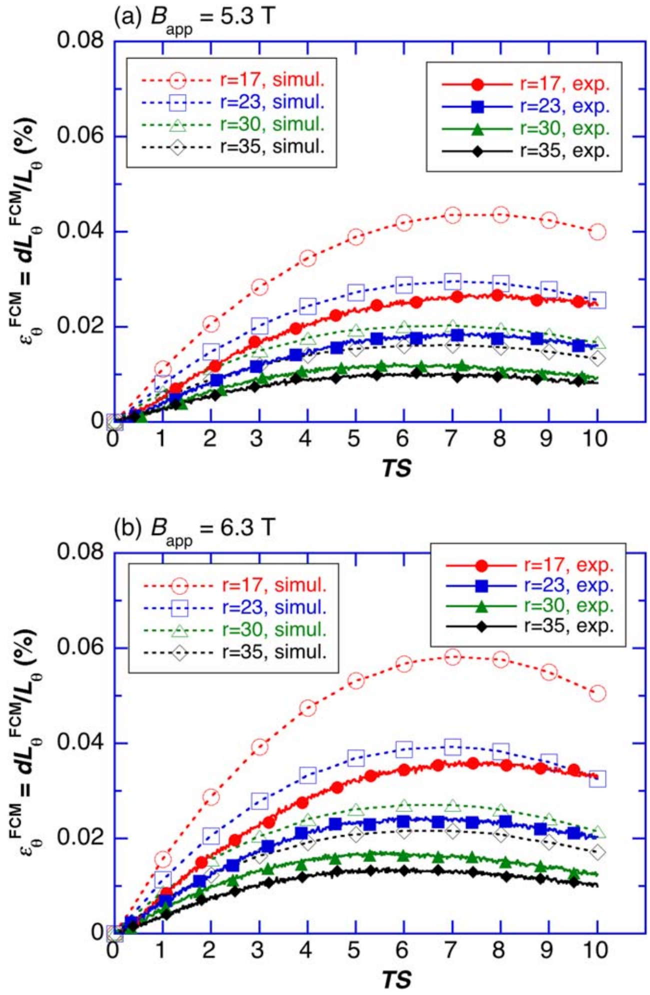

Figure 8. Experimental and numerical results of the time step dependence of the magnetic strain, $\varepsilon_\theta^{FCM} = dL_\theta^{FCM}/L_\theta$, during FCM from (a) $B_{app} = 5.3$ T and (b) 6.3 T at each measurement position on the bulk surface ($z = 10$ mm).

in the experiments and numerical simulations, the ε_θ^{FCM} values rise with increasing TS, take a peak value around TS = 6–7, and then decrease with increasing TS. The maximum ε_θ^{FCM} value increases with increasing B_{app}. These results strongly suggest magnetic strain can be measured using strain gauges.

The absolute ε_θ^{FCM} values obtained experimentally were about 50% smaller than those of the simulations at each measuring position and B_{app}. The difference between the experiments and numerical simulations is larger than that in the $\varepsilon_\theta^{cool}$ value without magnetic field shown in figure 5(a). These results suggest that the difference mainly comes from the simulation results of the magnetic strain, which is closely related with the used $J_c(B)$ characteristics. In the present study, the used $J_c(B)$ characteristics shown in figure 3(a) were determined as an 'average $J_c(B)$ value' in the bulk by the fitting to the experimental results shown in figure 7. The electromagnetic stress and strain depend on the $J_c(B)$, that is, the stress and strain decrease with decreasing $J_c(B)$. In actual REBaCuO bulks, there exists the $J_c(B)$ distribution, in which higher $J_c(B)$ region exists only near the seed crystal and other region has relatively lower $J_c(B)$ [1, 24]. In this case, the ε_θ^{FCM} values estimated by the average $J_c(B)$ might be overestimated, compared to the experimental values.

The ring bulk was assumed to be homogeneous in this simulation, in which the strain exists axisymmetrically in the bulk. However, in the present ring bulk, there exists an inhomogeneous strain distribution, which comes from the existence of growth sector regions and growth sector boundaries, and also voids, small cracks, Ag and RE211 particles. In an inhomogeneous material, a region with a large strain might exist and, as a result, the region with a small strain also exists [11]. The finite size of the actual strain gauge may also influence on the accuracy of the ε_θ^{FCM} value.

In this study, we measured magnetic strain, ε_θ^{FCM}, only along the θ-direction. When we also measure the magnetic strain, ε_r^{FCM}, along the r-direction at the same positions as the ε_θ^{FCM} measured positions, we can experimentally estimate the magnetic stresses, σ_θ^{FCM} and σ_r^{FCM}, along the θ- and r-direction, respectively, and better confirm the validity of the numerical simulation.

5. Conclusion

In this study, we have measured the mechanical strain along the circumferential direction of the EuBaCuO ring bulk reinforced by an aluminum alloy ring, during both the cooling process from 289 K to 50 K and during FCM from 5.3 and 6.3 T at 50 K. To discuss the mechanical reinforcement effect of the aluminum alloy ring, we have performed numerical simulations for the ring bulk with realistic superconducting characteristics. The important results and conclusions are summarized as follows.

(1) The experimental results of the thermal strain under the cooling process, $\varepsilon_\theta^{cool} = dL_\theta^{cool}/L_\theta$, from 289 K to 50 K on the bulk surface validated our numerical results, for which the $\varepsilon_\theta^{cool}$ value was getting smaller at the outer edge of the bulk surface, compared to that at the inner edge of the bulk surface. These results strongly suggest an inhomogeneous reinforcement on the bulk due to the difference in thermal contraction along the z-direction between the bulk and the outer Al ring with finite height.
(2) Using the electromagnetic simulation, the magnetic field dependence of the average critical current density, $J_c(B)$, can be deduced by the numerical fitting of the TS dependence of the trapped field, B_z(TS), to the experimentally obtained B_z(TS), which was measured at the center of the ring bulk.
(3) The experimental results of the TS dependence of the magnetic strain during FCM, $\varepsilon_\theta^{FCM} = dL_\theta^{FCM}/L_\theta$, and the applied field and position dependences of ε_θ^{FCM} were reproduced qualitatively by the numerical simulation. However, the experimental ε_θ^{FCM} values were about 50% smaller than those of the simulation. The difference mainly comes from the simulation results

of the magnetic strain, which is closely related with the used $J_c(B)$ characteristics. The existence of the macroscopic and microscopic structural inhomogeneity may also affect the ε_θ^{FCM} value.

(4) When both the magnetic strains, ε_θ^{FCM} and ε_r^{FCM}, along the θ- and r-directions at the same positions are measured using this technique, the magnetic stresses, σ_θ^{FCM} and σ_r^{FCM}, can be experimentally estimated and the validity of the numerical simulation can be confirmed.

Acknowledgments

This research is partially supported by a 'Development of Systems and Technologies for Advanced Measurement and Analysis' from Japan Agency for Medical Research and development, AMED and by JSPS KAKENHI grant no. JP15K04646. The Authors thank Dr Mark D Ainslie of University of Cambridge and Professor Fumihito Nishimura of Iwate University for valuable suggestions about the numerical simulation of the mechanical properties.

ORCID iDs

H Fujishiro https://orcid.org/0000-0003-1483-835X
T Naito https://orcid.org/0000-0001-7594-3466
T Nakamura https://orcid.org/0000-0002-8278-2688

References

[1] Shi Y-H, Namburi D K, Zhao W, Durrell J H, Dennis A R and Cardwell D A 2016 *Supercond. Sci. Technol.* **29** 015010
[2] Namburi D K, Shi Y-H, Palmer K G, Dennis A R, Durrell J H and Cardwell D A 2016 *Supercond. Sci. Technol.* **29** 034007
[3] Durrell J H *et al* 2014 *Supercond. Sci. Technol.* **27** 082001
[4] Nakamura T, Itoh Y, Yoshikawa M, Oka T and Uzawa J 2007 *Concepts Magn. Reson.* B **31B** 65–70
[5] Nakamura T, Tamada D, Yanagi Y, Itoh Y, Nemoto T, Utsumi H and Kose K 2015 *J. Magn. Reson.* **259** 68–75
[6] Ogawa K, Nakamura T, Terada Y, Kose K and Haishi T 2011 *Appl. Phys. Lett.* **98** 234101
[7] Itoh Y, Yanagi Y and Nakamura T 2017 *TEION KOGAKU (J. Cryog. Supercond. Soc. Japan.)* **52** 25–32 (in Japanese)
[8] Fujishiro H, Itoh Y, Yanagi Y and Nakamura T 2015 *Supercond. Sci. Technol.* **28** 095018
[9] Tomita M and Murakami M 2003 *Nature* **421** 517–20
[10] Ren Y, Weinstein R, Liu J, Sawh R P and Foster C 1995 *Physica* C **251** 15–26
[11] Miyamoto T, Nagashima K, Sakai N and Murakami M 2000 *Physica* C **340** 41–50
[12] Murakami A, Katagiri K, Kasaba K, Shoji Y, Noto K, Teshima H, Sawamura M and Murakami M 2002 *TEION KOGAKU (J. Cryog. Supercond. Soc. Japan.)* **37** 665–70 (in Japanese)
[13] Kasaba K, Oshida Y, Hokari T and Katagiri K 2008 *Physica* C **468** 1415–8
[14] Lee D and Salama K 1990 *Japan. J. Appl. Phys.* **29** L2017–9
[15] Matsui M, Sakai N and Murakami M 2002 *Supercond. Sci. Technol.* **15** 1092–8
[16] Katagiri K, Murakami A, Kan R, Kasaba K, Noto K, Muralidhar M, Sakai N and Murakami M 2003 *Physica* C **392–396** 526–30
[17] Fujishiro H, Ainslie M D, Takahashi K, Naito T, Yanagi Y, Itoh Y and Nakamura T 2017 *Supercond. Sci. Technol.* **30** 085008
[18] Takahashi K, Fujishiro H, Naito T, Yanagi Y, Itoh Y and Nakamura T 2017 *Supercond. Sci. Technol.* **30** 115006
[19] Morita M, Sawamura M, Takebayashi S, Kimura K, Teshima H, Tanaka M, Miyamoto K and Hashimoto M 1994 *Physica* C **235–240** 209–12
[20] Sawamura M, Morita M and Hirano H 2003 *Physica* C **392–396** 531–4
[21] Ainslie M D and Fujishiro H 2015 *Supercond. Sci. Technol.* **28** 053002
[22] Muralidhar M, Sakai N, Jirsa M, Koshizuka N and Murakami M 2004 *Appl. Phys. Lett.* **85** 3504
[23] Jirsa M, Půst L, Dlouhý D and Koblischka M R 1997 *Phys. Rev.* B **55** 3276–84
[24] Ainslie M D, Fujishiro H, Mochizuki H, Takahashi K, Shi Y-H, Namburi D K, Zhou D, Dennis A R and Cardwell D A 2016 *Supercond. Sci. Technol.* **29** 074003